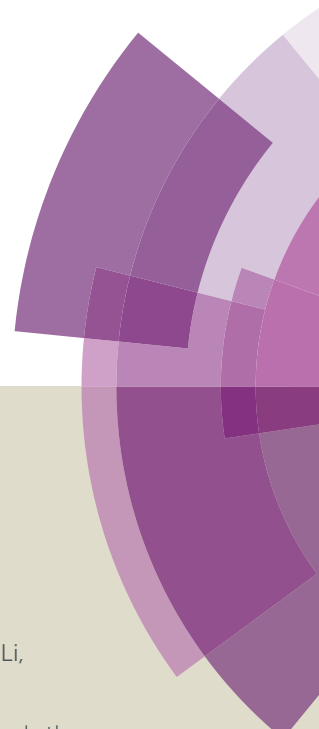


# Journal of Materials Chemistry A

Accepted Manuscript



This article can be cited before page numbers have been issued, to do this please use: H. Bai, W. Yi, J. Li, G. Xi, Y. Li, H. Yang and J. Liu, *J. Mater. Chem. A*, 2015, DOI: 10.1039/C5TA08603E.



This is an *Accepted Manuscript*, which has been through the Royal Society of Chemistry peer review process and has been accepted for publication.

*Accepted Manuscripts* are published online shortly after acceptance, before technical editing, formatting and proof reading. Using this free service, authors can make their results available to the community, in citable form, before we publish the edited article. We will replace this *Accepted Manuscript* with the edited and formatted *Advance Article* as soon as it is available.

You can find more information about *Accepted Manuscripts* in the [Information for Authors](#).

Please note that technical editing may introduce minor changes to the text and/or graphics, which may alter content. The journal's standard [Terms & Conditions](#) and the [Ethical guidelines](#) still apply. In no event shall the Royal Society of Chemistry be held responsible for any errors or omissions in this *Accepted Manuscript* or any consequences arising from the use of any information it contains.



Journal Name

COMMUNICATION

## Direct growth of defects-rich MoO<sub>3-x</sub> ultrathin nanobelts for efficiently catalyzed conversion of isopropyl alcohol to propylene under visible light

Received 00th January 20xx,  
Accepted 00th January 20xx

DOI: 10.1039/x0xx00000x

Hua Bai,<sup>a</sup> Wencai Yi,<sup>b</sup> Junfang Li,<sup>a</sup> Guangcheng Xi,<sup>\*a</sup> Yahui Li,<sup>a</sup> Haifeng Yang<sup>a</sup> and Jingyao Liu<sup>\*b</sup>

www.rsc.org/

**We report a robust and highly active photocatalyst for C<sub>3</sub>H<sub>8</sub> evolution reaction that is constructed by surfactant-free growth of oxygen vacancy-rich MoO<sub>3-x</sub> ultrathin nanobelts. Under visible-light irradiation, the new catalyst can selectively (95% selectivity) dehydrate isopropyl alcohol into C<sub>3</sub>H<sub>6</sub> with yields above 98 %.**

Propylene is one of the most important raw materials for chemical industry. Currently, catalytic or steam cracking of fossil feedstocks is the most commonly used method for the preparation of propylene in industry. However, with the increasing demands for energy and the depletion of non-renewable fossil feedstocks, more and more attention has been paid to alternative and renewable sources for fuels and chemicals. It is known that alcohols, such as ethanol, propanol, and isopropyl alcohol can be easily prepared by the biomass conversion technology.<sup>1-3</sup> Such biomass conversion technology offers inexhaustible energy source since plants as the raw materials are renewable. With increased availability and reduced cost of bio-alcohols, conversion of the bio-based feedstocks to highly valuable fuels and chemicals has been an especially important research issue.<sup>4,5</sup> Currently, research on alcohol conversion to value-added chemicals focuses mainly on ethanol dehydration to ethylene, or ethanol dehydrogenation to acetaldehyde and then to acetone via Aldol-condensations pathways, while for other types of alcohol dehydration have rarely been reported.<sup>6</sup> Generally, high reaction temperature (200–400 °C) are necessary in these reported methods.

Inorganic nanostructures with ultrathin diameter or thickness (less than 2 nm) and even one unit cell size, have attracting much research attention in the past few years,

owing to their unique chemical and physical properties.<sup>7-12</sup> Orthorhombic phase molybdenum oxide has been recognized as one of the most promising semiconductor materials for applications in lithium batteries, sensors, light-emitting diodes, and photocatalysts owing to its unique layered structure and environmental friendliness.<sup>13-15</sup> In particular, oxygen vacancies-rich MoO<sub>3-x</sub> is of great interest owing to its unusual oxygen defect structure and novel properties in the nanometer regime.<sup>16,17</sup> Since Wang et al. reported the synthesis of ultrathin MoO<sub>3-x</sub> single-wall nanotubes with a diameter of 6 nm by a thiol-assisted hydrothermal method,<sup>18</sup> ultrathin MoO<sub>3-x</sub> one-dimensional and two-dimensional nanostructures have been prepared by various solution-phase methods, such as bioligand- and surfactant-assisted routes.<sup>19-21</sup> However, complete removal of the surfactant or organic ligand molecules from the ultrathin nanostructure surface is almost impossible. For both fundamental investigations on the ultrathin nanostructure itself and technological applications, the presence of residue from the synthesis on the surface may be a significant drawback.<sup>22</sup> It can be predicted that researchers will have opportunity to research the natural chemical and physical properties of nanoscaled MoO<sub>3-x</sub> raised by oxygen vacancies once the ultrathin nanostructures with clear surfaces are received.

In this communication, we report the clean preparation of ultrathin MoO<sub>3-x</sub> nanobelts that are efficient in the photocatalytic conversion of isopropyl alcohol to propylene by visible light. The ultrathin MoO<sub>3-x</sub> Nanobelts were prepared by a simple one-pot solution-phase method (see the experimental section). In a typical procedure, molybdenum acetylacetonate was dissolved in distilled water, and the obtained solution was transferred to a teflon-lined stainless-steel autoclave and heated at 180 °C for 20 h. A blue flocculent precipitate was collected, washed, dried in air, and obtained in a yield of approximately 100%. The product is insoluble in water and in acid (HCl, pH 0), and has a high specific surface area of 201 m<sup>2</sup>/g (Figure S1).

The most important structural characteristic of orthorhombic phase molybdenum oxide is its structural

<sup>a</sup>Nanomaterials and Nanoproducts Research Center, Chinese Academy of Inspection and Quarantine, No. 11, Ronghua South Road, Beijing, 100123, China. Email: xiguangcheng@caiq.gov.cn

<sup>b</sup>International Joint Research Laboratory of Nano-Micro Architecture Chemistry, Institute of Theoretical Chemistry, Jilin University, Changchun 130023, P. R. China. Electronic Supplementary Information (ESI) available: Experimental procedure, XRD patterns, TEM and HRTEM images, energy-dispersive X-ray spectra, UV-vis spectra, X-ray photoelectron spectroscopy (XPS), and EDS. See DOI: 10.1039/x0xx00000x

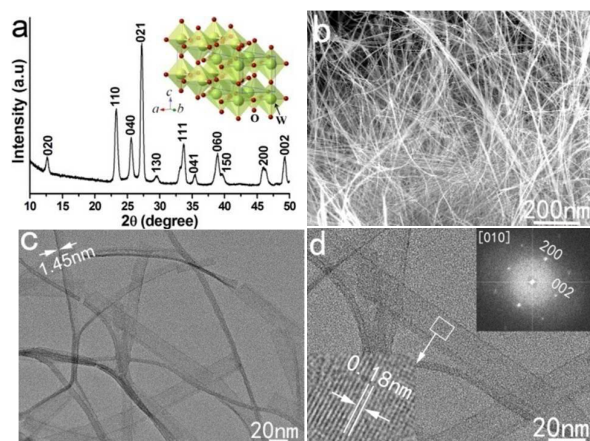


**Figure 1.** (a) XRD pattern of the as-prepared  $\text{MoO}_{3-x}$  sample, inset: crystal structure of orthorhombic molybdenum oxide. (b,c) SEM and TEM images of the ultrathin  $\text{MoO}_{3-x}$  nanobelts. (d) HRTEM image and corresponding FFT pattern of the ultrathin nanobelts.

anisotropy (inset in Figure 1a), which can be considered as a layered structure parallel to (010). Distorted  $\text{MoO}_6$  octahedra are four corners to form a plane and two planes join together by sharing octahedral edges to form a single layer. The layers stack up along the [010] direction by van der Waals forces. The high crystallinity and phase purity of the resultant samples were confirmed by XRD (Figure 1a). Our XRD pattern is consistent with previous reports.<sup>15-17</sup> The diffraction peaks of the XRD pattern for the sample can be readily indexed to be orthorhombic with lattice constants of  $a = 3.962 \text{ \AA}$ ,  $b = 13.85 \text{ \AA}$ ,  $c = 3.697 \text{ \AA}$  (JCPDs, No. 05-0508). No peaks of any other crystalline phases were detected, indicating the high purity of the  $\text{MoO}_{3-x}$  ultrathin nanobelts.

Scanning electron microscopy (SEM) image shows that the as-synthesized sample is composed of 1D nanostructures with large aspect ratio and lengths of up to several micrometers (Figure 1b). Transmission electron microscope (TEM) image shows that the as-synthesized 1D nanostructures are composed of ultrathin  $\text{MoO}_{3-x}$  nanobelts with width of 20-30 nm and lengths of up to several micrometers (Figure 1c). From the vertical view (marked by arrows in Figure 1c), the standing ultrathin  $\text{MoO}_{3-x}$  nanobelts show a wire-like morphology due to its ultrathin thickness. The thickness of the nanobelts is only about 1.45 nm. The high-resolution TEM (HRTEM) image (Figure 1d) shows that the ultrathin  $\text{MoO}_{3-x}$  nanobelts are highly crystallized. The fringe spacing of 0.18 nm (shown in the inset of Figure 1d) agrees well with the spacing of the (002) plane of orthorhombic  $\text{MoO}_3$ . The diffraction spots of the corresponding FFT pattern (indexed as the [010] zone) can be indexed as the 200 and 002 reflections (inset of Figure 1d), clearly demonstrating that the growth direction of the nanobelts is [001], the top/bottom surfaces of the belts are (010) and the side surfaces are (100). Energy-dispersive X-ray spectroscopy (EDS) confirms that the sample only contains Mo and O elements (Figure S2). Furthermore, the Fourier transform infrared (FTIR) spectrum exhibits the clear surface of our sample (Figure S3).

The ultrathin  $\text{MoO}_{3-x}$  nanobelts show unusual photophysical properties, as indicated by ultraviolet–visible–near infrared (UV–Vis–NIR) absorption spectroscopy (Figure 2a). It is well known that commercial  $\text{MoO}_3$  with a wide band gap (3.1 eV) requires high-energy UV light to activate it. However, a very strong absorption peak with a center of 550 nm present in the visible and near infrared regions of the absorption spectrum gives clear evidence that the  $\text{MoO}_{3-x}$  nanobelts consist of a large number of oxygen vacancies,<sup>22</sup> which is also demonstrated by electron spin resonance (ESR) spectrum (Figure S4). This result is very different from those 1D and 2D  $\text{MoO}_{3-x}$  nanostructures synthesized by surfactant-assisted methods.<sup>18,20</sup> For those  $\text{MoO}_{3-x}$  nanostructures obtained via surfactant-assisted methods, their absorption peaks often appear in the NIR infrared region.<sup>18,20</sup> It is also noted that Chen et al. reported the surfactant-free synthesis of 20–30 nm thick  $\text{MoO}_{3-x}$  nanosheets with a LSPR peak center at about 680 nm,<sup>23</sup> which may be the first observation of the visible LSPR in  $\text{MoO}_{3-x}$  nanostructures. Compared with the value reported by Chen et al., the result obtained by our experiments experienced a significant blue shift of 130 nm. To the best of our knowledge, the strong absorption below 600 nm wavelength has not been reported for molybdenum oxide. Moreover, this absorption peak may be the shortest wavelength of semiconductor LSPR even though compared with other typical plasmonic semiconductor nanostructures (such as  $\text{CuS}_{2-x}$ ,  $\text{CuSe}_{2-x}$ ,  $\text{CuTe}_{2-x}$ ,  $\text{WO}_{3-x}$ ,  $\text{TiO}_{2-x}$ , Al-ZnO, and Si) which usually appear in the NIR–mid infrared (MIR) region (Table S1 in Supporting Information).<sup>25-33</sup> From the view point of energy conversion, the visible-LSPRs with higher energy are more promising and efficient way compared with the NIR-LSPRs.

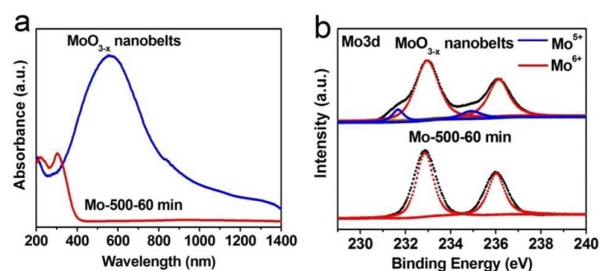


**Figure 2.** a) UV-Vis-NIR absorption spectrum and b) Mo3d XPS spectra of the oxygen vacancies-rich  $\text{MoO}_{3-x}$  ultrathin nanobelts and Mo-500-60 min.

We speculate this significant blue shift of LSPR absorption peak may be attributed to its very high concentration oxygen vacancies contained in the ultrathin  $\text{MoO}_{3-x}$  nanobelts. Control experiments show that the color of a  $\text{MoO}_{3-x}$  sample gradually changed from vivid blue in the original sample to white in the final sample (Figure S5) once the sample was oxidized by heating the  $\text{MoO}_{3-x}$  nanobelts in air at 500 °C for 60 min. The corresponding absorption spectrum of the white sample (marked as Mo-500-60 min) shows a little red shift, and no absorption is present in the visible and near infrared regions, which indicates that the oxygen vacancies contained in the nanobelts disappear after oxidizing with heated air. In

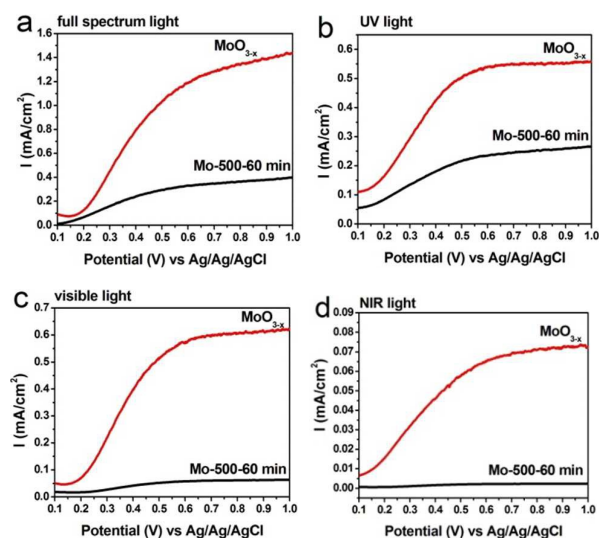


**Figure 3.** Photocurrent response of the oxygen vacancies-rich  $\text{MoO}_{3-x}$  ultrathin nanobelts under the illumination of (a) full-spectrum light (200–2000 nm), (b) UV light (200–420 nm), (c) visible light (420–780 nm), and (d) NIR light (780–2000 nm).

contrast, after the oxygen vacancy concentration of the  $\text{MoO}_{3-x}$  ultrathin nanobelts was increased by  $\text{NaBH}_4$  reduction, a stronger visible-LSPR peak located at 516 nm was detected (Figure S6). The change in the valence of Mo atoms in the ultrathin nanobelt surface before and after oxidation could be further characterized by using X-ray photoelectron spectroscopy (XPS; Figure 2b). For the  $\text{MoO}_{3-x}$  ultrathin nanobelts, four peaks corresponding to Mo3d could be seen in the XPS spectrum. Two peaks observed at 232.8 and 235.9 eV correspond to  $\text{Mo}^{6+}$ , and the other two peaks at 231.9 and 234.9 eV are assigned to  $\text{Mo}^{5+}$ .<sup>20</sup> For the sample Mo-500-60 min, two sharp peaks of Mo3d can be seen in the spectrum, which is a typical feature of  $\text{Mo}^{6+}$ . At the same time, two peaks can also be clearly identified from the O1s core level spectra shown in Figure S7: one peak at 529.8 eV is deemed as the oxygen bond of Mo–O–Mo, while the other located at 531.4 eV can be attributed to the O-atoms in the vicinity of an O-vacancy.<sup>34</sup> As for the Mo-500-60 min, no obvious O-vacancy mode was detected. The XPS spectra clearly demonstrated that after oxidizing with heated air, the valence of Mo has completely changed into  $\text{Mo}^{6+}$ . This means that the oxygen vacancies contains in the ultrathin nanobelts disappeared after oxidation with heated air, which also explains the disappearing of the absorption peak in the absorption spectra.

The photoelectrochemical properties of the ultrathin  $\text{MoO}_{3-x}$  nanobelts are examined by means of photocurrent responses. We measured the photocurrent response in a three-electrode electrochemical cell with Ag/AgCl as the reference electrode and Pt wire as the counter electrode (see Experimental Section in Supporting Information). The photocurrent responses for all samples under dark are very low, while obvious current responses could be discerned from 0.1 to 1.0 eV (vs Ag/AgCl) under full-spectrum light (Fig. 3a). The ultrathin  $\text{MoO}_{3-x}$  nanobelts show the higher photocurrent density compared

with the Mo-500-60 min, indicating that  $\text{MoO}_{3-x}$  ultrathin nanobelts should be better semiconductor material for solar light harvesting. For a better understanding on the light harvesting by  $\text{MoO}_{3-x}$  ultrathin nanobelts, the photocurrent responses under different illumination conditions are examined. Under UV or visible light, the  $\text{MoO}_{3-x}$  nanobelts also show the higher photocurrent density compared with Mo-500-60 min (Figure 3b–c). The enhanced photocurrent responses of  $\text{MoO}_{3-x}$  ultrathin nanobelts as compared with Mo-500-60 min should be related to the introduction of oxygen vacancies. As an evidence, photoluminescence (PL) spectra recorded at an excitation wavelength of 300 nm demonstrated this hypothesis (Figure S8). The PL emission spectrum of the  $\text{MoO}_{3-x}$  ultrathin nanobelts recorded at  $-10^\circ\text{C}$  shows a strong blue emission band at 2.87 eV (435 nm), which originate from the presence of oxygen vacancies or defects. Figure S8 also reveals that the ultrathin  $\text{MoO}_{3-x}$  nanobelts lower PL intensity compared with the Mo-500-60 min, suggesting the recombination of photo-generated electron-hole pairs is effectively suppressed upon the introduction of oxygen vacancies, which accordingly results in higher photocurrent responses.<sup>35</sup> Very interestingly, the  $\text{MoO}_{3-x}$  ultrathin nanobelts also show noticeable photocurrent responses under near-infrared illumination, in great contrast to Mo-500-60 min (Figure 3d). The observed photocurrent responses under near-infrared illumination should come from LSPR induced by the abundant oxygen vacancies. On the basis of photocurrent responses under different illumination conditions, we could come to the conclusion the introduction of oxygen vacancies to molybdenum oxide nanobelts can not only promote full-spectrum, UV, and visible light harvesting but also create near-infrared light harvesting.

Because crystal defects often give rise to unexpected results in chemical reactions, we investigated the photochemical activity of the oxygen-vacancy-rich  $\text{MoO}_{3-x}$  nanobelts by the photochemical dehydration of isopropyl alcohol (IPA,  $\text{CH}_3\text{CH}(\text{OH})\text{CH}_3$ ) vapor in a gas-solid system. The ultrathin  $\text{MoO}_{3-x}$  nanobelts achieved efficient propylene ( $\text{C}_3\text{H}_6$ ) production from isopropyl alcohol vapor on illumination with visible light ( $\lambda > 420\text{ nm}$ ) in the absence of noble-metal co-catalysts such as Pt and Au (Figure 4a). The average formation rate of  $\text{C}_3\text{H}_6$  is about  $5.75\text{ mmol g}^{-1}\text{h}^{-1}$ . Besides  $\text{C}_3\text{H}_6$ , only 3% (molar ratio) of other compounds (such as carbon dioxide and acetone) were produced, which suggests that the selectivity of this photochemical reaction is very high. Because the equilibrium temperature of the photochemical reaction system was about  $50^\circ\text{C}$ , control experiments were carried out to detect the influence of temperature on product formation. The experimental results indicated that only very small amount of  $\text{C}_3\text{H}_6$  (0.18 mmol g<sup>-1</sup>h<sup>-1</sup>) was detected when the reactions were performed in the dark at  $50^\circ\text{C}$ , that is, the dehydration of isopropyl alcohol almost cannot be started in the absence of light. To further support that the present catalytic reaction proceeds through light absorption within ultrathin  $\text{MoO}_{3-x}$  nanobelts, we also examined the dependence of the rate of  $\text{C}_3\text{H}_6$  evolution on the wavelength of incident light. As shown in Figure S9, the maximum of  $\text{C}_3\text{H}_6$  evolution rates is obtained when 540 nm incident light was used, which

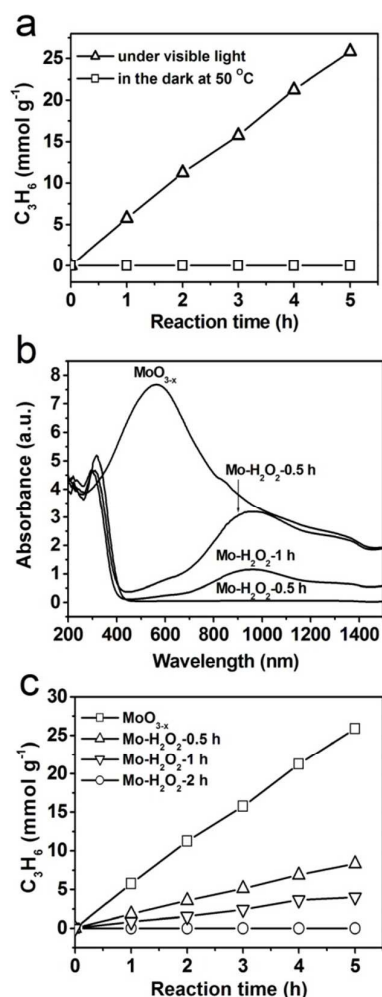


**Figure 4.** (a) Time courses of C<sub>3</sub>H<sub>6</sub> production over the as-synthesized MoO<sub>3-x</sub> ultrathin nanobelts under visible light ( $\lambda > 420$  nm) and in the dark at 50 °C. (b) UV/Vis absorption spectra of the molybdenum oxide samples obtained by oxidation with H<sub>2</sub>O<sub>2</sub> for different time periods. (c) Time courses of C<sub>3</sub>H<sub>6</sub> production over the molybdenum oxide samples with different oxygen-vacancy concentrations.

is a high match with the LSPR central wavelength. Therefore, the formation of C<sub>3</sub>H<sub>6</sub> is really based on a photopromoted dehydration of isopropyl alcohol. To our knowledge, the photochemical conversion of isopropyl alcohol into C<sub>3</sub>H<sub>6</sub> over MoO<sub>3-x</sub> under visible light has not been reported to date.

We then investigated the effect of the concentration of oxygen vacancies on the photochemical dehydration of isopropyl alcohol. By adjusting the H<sub>2</sub>O<sub>2</sub> treating time, a series of molybdenum oxide samples with different oxygen-vacancy concentrations was prepared. UV-Vis-NIR absorption spectra show the oxygen-vacancy concentrations of the samples gradually reduced as the oxidation time increased (Figure 4b). Figure 4c shows the rate of C<sub>3</sub>H<sub>6</sub> evolution on molybdenum oxide catalysts with different concentrations of oxygen vacancies. After oxidizing for 0.5 h, the activity of C<sub>3</sub>H<sub>6</sub> evolution on the sample is reduced down to 32% (1.84 mmol g<sup>-1</sup> h<sup>-1</sup>). After oxidizing for 1 h, the sample still shows activity in photochemical C<sub>3</sub>H<sub>6</sub> evolution, but the rate of C<sub>3</sub>H<sub>6</sub> evolution is

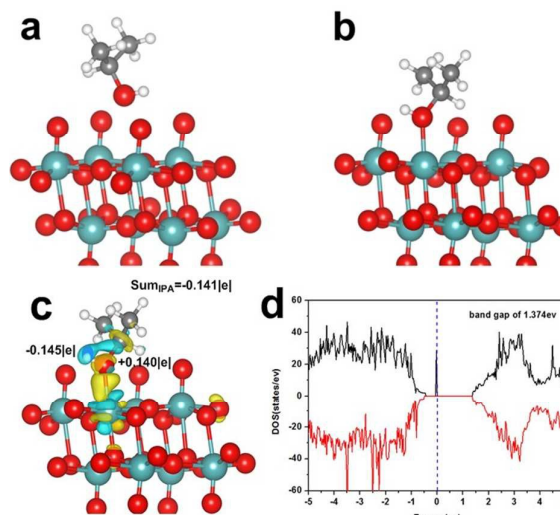


**Figure 5.** Adsorption structure of isopropyl alcohol on (a) MoO<sub>3</sub> nanobelts and (b) on MoO<sub>3-x</sub> nanobelts; (c) Charge-density difference for isopropyl alcohol adsorption on the MoO<sub>3-x</sub> nanobelts, Isosurfaces calculated at 0.004e/Å<sup>3</sup>; (d) DOS of MoO<sub>3-x</sub> after isopropyl alcohol adsorption.

very lower (0.85 mmol g<sup>-1</sup> h<sup>-1</sup>). Finally, no C<sub>3</sub>H<sub>6</sub> were detected when Mo-H<sub>2</sub>O<sub>2</sub>-2 h was used as the catalyst, the surface of which was completely oxidized into Mo<sup>6+</sup> by H<sub>2</sub>O<sub>2</sub> (Figure S10), thus suggesting that MoO<sub>3</sub> is not active for photocatalytic C<sub>3</sub>H<sub>6</sub> evolution. These experimental results demonstrated unambiguously that oxygen vacancies in the samples play a very important role in the photocatalytic C<sub>3</sub>H<sub>6</sub> evolution under visible light.

In order to clarify the underlying mechanism for the high photochemical activity of the ultrathin MoO<sub>3-x</sub> nanobelts, we also studied the isopropyl alcohol adsorption structures and energies on the ultrathin MoO<sub>3-x</sub> nanobelts at the DFT+U level (see Supporting Information of adsorption energies calculations for details, Figure S11-12). Seen from Figure 5a, isopropyl alcohol is weakly physisorbed over the perfect MoO<sub>3</sub> nanobelts, with adsorption energy of -0.10 eV and no strong preference for a particular surface site. While as the creation of an O-vacancy on molybdenum oxide nanobelt, Mo<sup>5+</sup> is exposed, which leads to a much stronger adsorption of isopropyl alcohol molecule through O at the defect site of MoO<sub>3-x</sub> nanobelt (Figure 5b). The calculated adsorption energy becomes -1.29 eV. At the same time, the greatly enhanced adsorption make the C-O bond length of isopropyl alcohol increase of 0.047 Å, reaching 1.487 Å, which reduce the breaking energy of carbon-oxygen bond of isopropyl alcohol. Furthermore, the plot of the contour surface of the charge-density difference for the isopropyl alcohol adsorption is shown in Figure 5c. The further Bader charge analysis suggests that the electrons are transferred from the hydrogen to oxygen in hydroxyl of isopropyl alcohol and from IPA to surface. The charge-charge interaction between isopropyl alcohol and MoO<sub>3-x</sub> may account for the enhanced adsorption ability of isopropyl alcohol. In addition, the band gap of the ultrathin MoO<sub>3-x</sub> nanobelt is further reduced from 1.917 eV before isopropyl alcohol adsorption to 1.374 eV after isopropyl

alcohol adsorption (Figure 5d), consistent with the high activity of MoO<sub>3-x</sub> nanobelt observed in experiments.

Based on the experimental and calculated results, it can be rationally concluded that the oxygen vacancies contained in the ultrathin nanobelts play a crucial role in the formation of C<sub>3</sub>H<sub>6</sub>, which may markedly increase the number of catalytically active sites on their surfaces and facilitate the adsorption of organic molecules on these sites. From the point of view of catalytic kinetics, the stronger adsorption between oxygen vacancy and isopropyl alcohol molecule may generate unexpected affinity interaction, and therefore, reduces the reactive barrier of the dehydration reaction. At the same time, the strong LSPR effect result from the large quantity of oxygen vacancies make the oxygen vacancies-rich MoO<sub>3-x</sub> nanobelts highly efficient photocatalytic conversion agent. As we know, the instantaneous temperature of LSPRs can reach 1000K,<sup>35</sup> which offers enough energy for the isopropyl alcohol dehydration reaction.

To evaluate stability of the MoO<sub>3-x</sub> ultrathin nanobelts, the reaction was allowed to proceed for a total 30 h with intermittent evacuation every 5 h. Continuous C<sub>3</sub>H<sub>6</sub> evolution with no apparent decrease in its photocatalytic activity was clearly observed (Figure S13). After the reactions, the structure and morphology of the catalysts is not apparently change (Figure S14-15).

## Conclusions

In summary, ultrathin MoO<sub>3-x</sub> nanobelts were successfully synthesized by a very simple one-pot solution method. The ultrathin nanobelts contain a large number of oxygen vacancies, which lead them to possess much strong visible-LSPR absorption and greatly enhanced photocurrent responses under UV light, visible light, and even NIR light irradiation. As a result, the oxygen vacancy-rich MoO<sub>3-x</sub> nanobelts show a remarkable capability of photocatalytic dehydration of isopropyl alcohol into C<sub>3</sub>H<sub>6</sub> under visible light irradiation. This work presents not only a possibility for the use of ultrathin MoO<sub>3-x</sub> nanobelts as a efficient photocatalyst in the synthetic chemistry of olefins but also an important concept that oxygen-vacancy-rich nonstoichiometric simple oxides can be used as a new strategy to design materials with high light harvesting and photocatalytic activity.

## Notes and references

- J. Goldemberg, *Science* **2007**, *315*, 808.
- G. W. Huber, S. Iborra, A. Corma, *Chem. Rev.* **2006**, *106*, 4044.
- J. N. Chheda, J. A. Dumesic, *Catal. Today* **2007**, *123*, 59.
- G. A. Deluga, J. R. Salge, L. D. Schmidt, X. E. Verykios, *Science* **2004**, *303*, 993.
- I. Takahara, M. Saito, M. Inaba, K. Murata, *Catal. Lett.* **2005**, *105*, 64.
- a) J. M. Sun, K. K. Zhu, F. Gao, C. M. Wang, J. Liu, C. H. F. Peden, Y. Wang, *J. Am. Chem. Soc.* **2011**, *133*, 11096–11099; b) P. Liu, E. J. M. Hensen, *J. Am. Chem. Soc.* **2013**, *135*, 14032–14035; c) J. M. Sun, Y. Wang, *ACS Catal.* **2014**, *4*, 1078–1090; d) X. Q. Huang, S. H. Tang, X. L. Mu, Y. Dai, G. X.

- Chen, Z. Y. Zhou, F. X. Ruan, Z. L. Yang, N. F. Zheng, *Nat. Nanotechnol.* **2011**, *6*, 28–32.
- Y. F. sun, Z. H. sun, s. Gao, H. Cheng, Q. H. Liu, J. Y. Piao, T. Yao, C. Z. Wu, S. L. Hu, S. Q. Wei, Y. Xie, *Nat. Commun.* **2012**, *3*, 1057.
- H. H. Duan, N. Yan, R. Yu, C. R. Chang, G. Zhou, H. S. Hu, H. P. Rong, Z. Q. Niu, J. J. Mao, H. Asakura, T. Tanaka, P. J. Dyson, J. Li1, Y. D. Li, *Nat. Commun.* **2014**, *5*, 3093.
- H. H. Li, S. Zhao, M. Gong, C. H. Cui, D. He, H. W. Liang, L. Wu, S. H. Yu, *Angew. Chem. Int. Ed.* **2013**, *52*, 7472–7476.
- S. Hu, H. L. Liu, P. P. Wang, X. Wang, *J. Am. Chem. Soc.* **2013**, *135*, 11115–11124.
- a) L. Q. Mai, B. Hu, W. Chen, Y. Y. Qi, C. S. Lao, R. Yang, Y. Dai, Z. L. Wang, *Adv. Mater.* **2007**, *19*, 3712–3716.
- a) J. He, H. I. Liu, B. Xu, X. Wang, *Small* **2014**, *11*, 1144–1149; b) S. Hu, X. Wang, *Chem. Soc. Rev.* **2013**, *42*, 5577–5594.
- Z. Y. Yin, X. Zhang, Y. Q. Cai, J. Chen, J. I. Wong, Y. Y. Tay, J. W. Chai, J. Wu, Z. Y. Zeng, B. Zheng, H. Y. Yang, H. Zhang, *Angew. Chem. Int. Ed.* **2014**, *53*, 12560–12565.
- S. Balendhran, S. Walia, H. Nili, J. Z. Ou, S. Zhuiykov, R. B. Kaner, S. Sriram1, M. Bhaskaran, K. Kalantar-zadeh, *Adv. Funct. Mater.* **2013**, *23*, 3952–3970.
- X. W. Lou, H. C. Zeng, *J. Am. Chem. Soc.* **2003**, *125*, 2697–2704.
- N. Pinna, M. Niederberger, *Angew. Chem. Int. Ed.* **2008**, *47*, 5292–5304.
- S. Hu, X. Wang, *J. Am. Chem. Soc.* **2008**, *130*, 8126–8127.
- S. Balendhran, S. Walia, M. Alsaif, E. P. Nguyen, J. Z. Ou, S. Zhuiykov, S. Sriram, M. Bhaskaran, K. Kalantar-zadeh, *ACS Nano*, **2013**, *7*, 9753–9760.
- Q. Q. Huang, S. Hu, J. Zhuang, X. Wang, *Chem. Eur. J.* **2012**, *18*, 15283–15287.
- D. L. Chen, M. N. Liu, L. Yin, T. Li, Z. Yang, X. J. Li, B. B. Fan, H. L. Wang, R. Zhang, Z. X. Li, H. L. Xu, H. X. Lu, D. Y. Yang, J. Sune, L. Gao, *J. Mater. Chem.* **2011**, *21*, 9332–9342.
- J. A. Lopez-Sanchez1, N. Dimitratos, C. Hammond, G. L. Brett, L. Kesavan, S. White, P. Miedziak, R. Tiruvalam, R. L. Jenkins, A. F. Carley, D. Knight, C. J. Kiely, G. J. Hutchings, *Nat. Chem.* **2011**, *3*, 551–556.
- T. Nutz, M. Haase, *J. Phys. Chem. B* **2000**, *104*, 8430.
- H. F. Cheng, T. Kamegawa, K. Mori, H. Yamashita, *Angew. Chem. Int. Ed.* **2014**, *53*, 2910.
- J. M. Luther, P. K. Jain, T. Ewers, A. P. Alivisatos, *Nat. Mater.* **2011**, *10*, 361–366.
- D. Dorfs, T. Härtlin, K. Miszta, N. C. Bigall, M. R. Kim, A. Genovese, A. Falqui, M. Povia, L. Manna, *J. Am. Chem. Soc.* **2011**, *133*, 11175–11180.
- S. W. Hsu, K. On, A. R. Tao, *J. Am. Chem. Soc.* **2011**, *133*, 19072–19075.
- I. Krieger, C. Y. Jiang, J. Rodríguez-Fernández, R. D. Schaller, D. V. Talapin, E. da Como, J. Feldmann, *J. Am. Chem. Soc.* **2012**, *134*, 1583–1590.
- L. W. Chou, N. Shin, S. V. Sivaram, M. A. Filler, *J. Am. Chem. Soc.* **2012**, *134*, 16155–16158.
- K. Manthiram, A. P. Alivisatos, *J. Am. Chem. Soc.* **2012**, *134*, 3995–3998.
- G. C. Xi, S. X. Ouyang, P. Li, J. H. Ye, Q. Ma, N. Su, H. Bai, C. Wang, *Angew. Chem. Int. Ed.* **2012**, *51*, 2395–2399.
- T. R. Gordon, M. Cargnello, T. Paik, F. Mangolini, R. T. Weber, P. Fornasiero, C. B. Murray, *J. Am. Chem. Soc.* **2012**, *134*, 6751–6761.
- R. Buonsanti, A. Llordes, S. Aloni, B. A. Helms, D. J. Milliron, *Nano Lett.* **2011**, *11*, 4706–4710.
- F. C. Lei, Y. F. Sun, K. T. Liu, S. Gao, L. Liang, B. C. Pan, Y. Xie, *J. Am. Chem. Soc.* **2014**, *136*, 6826–6829.
- J. Q. Yan, T. Wang, G. J. Wu, W. L. Dai, N. J. Guan, L. D. Li, J. L. Gong, *Adv. Mater.* **2015**, *27*, 1580.

## COMMUNICATION

Journal Name

- 35 L. Tong, Y. Zhao, T. B. Huff, M. N. Hansen, A. Wei, J. X. Cheng, *Adv. Mater.* **2007**, *19*, 3136-3141.

Oxygen Vacancies-Rich  $\text{MoO}_{3-x}$  Ultrathin nanobelts with diameters less than 1.5 nm and aspect ratios larger than 1000 have been synthesized without using any surfactants. The as-synthesized ultrathin  $\text{MoO}_{3-x}$  nanobelts show remarkable capability in photocatalytic conversion of isopropyl alcohol to propylene depending on its high adsorption energy and strong localized surface plasmon resonance caused by large quantities of oxygen vacancies.

